Manoj Amrutkar,[1] Emmelie Cansby,[1] Urszula Chursa,[1] Esther Nuñez-Durán,[1] Belén Chanclón,[1] Marcus Ståhlman,[2] Vincent Fridén,[3] Louise Mannerås-Holm,[2] Anna Wickman,[3] Ulf Smith,[1] Fredrik Bäckhed,[2,4] Jan Borén,[2] Brian W. Howell,[5] and Margit Mahlapuu[1]

Genetic Disruption of Protein Kinase STK25 Ameliorates Metabolic Defects in a Diet-Induced Type 2 Diabetes Model

Diabetes 2015;64:2791–2804 | DOI: 10.2337/db15-0060

Understanding the molecular networks controlling ectopic lipid deposition, glucose tolerance, and insulin sensitivity is essential to identifying new pharmacological approaches to treat type 2 diabetes. We recently identified serine/threonine protein kinase 25 (STK25) as a negative regulator of glucose and insulin homeostasis based on observations in myoblasts with acute depletion of STK25 and in STK25-overexpressing transgenic mice. Here, we challenged *Stk25* knockout mice and wild-type littermates with a high-fat diet and showed that STK25 deficiency suppressed development of hyperglycemia and hyperinsulinemia, improved systemic glucose tolerance, reduced hepatic gluconeogenesis, and increased insulin sensitivity. *Stk25*$^{-/-}$ mice were protected from diet-induced liver steatosis accompanied by decreased protein levels of acetyl-CoA carboxylase, a key regulator of both lipid oxidation and synthesis. Lipid accumulation in *Stk25*$^{-/-}$ skeletal muscle was reduced, and expression of enzymes controlling the muscle oxidative capacity (*Cpt1*, *Acox1*, *Cs*, *Cycs*, *Ucp3*) and glucose metabolism (*Glut1*, *Glut4*, *Hk2*) was increased. These data are consistent with our previous study of STK25 knockdown in myoblasts and reciprocal to the metabolic phenotype of *Stk25* transgenic mice, reinforcing the validity of the results. The findings suggest that STK25 deficiency protects against the metabolic consequences of chronic exposure to dietary lipids and highlight the potential of STK25 antagonists for the treatment of type 2 diabetes.

Type 2 diabetes (T2D), characterized by hyperglycemia in the context of insulin resistance, affects at least 285 million individuals worldwide, and its prevalence is expected to continue to increase (1). T2D is strongly associated with obesity and pathological lipid deposition within nonadipose tissue, which is suggested to actively contribute to the development of insulin resistance (2–5). Therefore, a better understanding of the molecular networks controlling ectopic lipid storage and glucose and insulin homeostasis is important to identifying new pharmacological approaches to effectively prevent and treat T2D.

In the search for novel genes regulating glucose tolerance and insulin sensitivity, we identified serine/threonine protein kinase 25 (STK25) (also referred to as YSK1 or SOK1) as a new regulator of whole-body energy homeostasis (6–8). STK25 belongs to the sterile 20 (STE20) superfamily of kinases, with ~30 mammalian members described to date (9). STE20 kinases regulate a broad range of biological processes, such as cell differentiation and proliferation, apoptosis, polarity, stress responses, and cytoskeleton rearrangements (10). STK25 possesses a highly conserved N-terminal catalytic domain, a variable linker region, and a carboxylic acid terminal

[1]Lundberg Laboratory for Diabetes Research, Department of Molecular and Clinical Medicine, University of Gothenburg, Gothenburg, Sweden
[2]Wallenberg Laboratory, Department of Molecular and Clinical Medicine, University of Gothenburg, Gothenburg, Sweden
[3]Center for Physiology and Bio-Imaging, Core Facilities, Sahlgrenska Academy, University of Gothenburg, Gothenburg, Sweden
[4]The Novo Nordisk Foundation Center for Basic Metabolic Research, University of Copenhagen, Copenhagen, Denmark
[5]Department of Neuroscience and Physiology, State University of New York Upstate Medical University, Syracuse, NY

Corresponding author: Margit Mahlapuu, margit.mahlapuu@gu.se.

Received 13 January 2015 and accepted 31 March 2015.

This article contains Supplementary Data online at http://diabetes.diabetesjournals.org/lookup/suppl/doi:10.2337/db15-0060/-/DC1.

dimerization domain (11). In several cell types, STK25 is localized to the Golgi apparatus, where it functions in a signaling cascade regulating cell migration and polarization (12–15). In response to chemical anoxia and oxidant stress, STK25 exits the Golgi complex, inducing apoptotic cell death (16,17). We found that partial depletion of STK25 in the rat myoblast cell line L6 by small interfering RNA (siRNA) increases lipid oxidation and improves insulin-stimulated glucose uptake (6). Consistent with this finding, we observed higher *STK25* levels in the skeletal muscle of patients with T2D than in individuals with normal glucose tolerance (6). Furthermore, our studies showed that STK25-overexpressing transgenic mice develop hyperinsulinemia, reduced whole-body glucose tolerance, and impaired insulin sensitivity compared with wild-type littermates when both genotypes are fed a high-fat diet (7). STK25 is associated with hepatic lipid droplets, and the liver of *Stk25* transgenic mice displays markedly increased lipid deposition due to reduced hepatic fatty acid oxidation and triacylglycerol secretion (8). Of note, we observed focal fibrosis, hepatocellular damage, and inflammation in transgenic livers, whereas these signs of steatohepatitis are virtually absent in wild-type livers, suggesting that STK25 not only promotes hepatic lipid accumulation but also triggers progression from simple liver steatosis to nonalcoholic steatohepatitis (8).

On the basis of these previous findings, we hypothesized that depletion of STK25 at the whole-body level improves systemic glucose tolerance and insulin sensitivity. To elucidate the impact of STK25 inactivation in vivo, we characterized the metabolic profile of *Stk25* knockout mice and wild-type littermates challenged with a high-fat diet. The data suggest that depletion of STK25 protects against the metabolic consequences of chronic exposure to dietary lipids.

RESEARCH DESIGN AND METHODS

Animals

Stk25 mutant mice were generated by deletion of exons 4 and 5 and genotyped as previously described (Supplementary Fig. 1*A* and *B*) (18). Heterozygous mice were backcrossed to a C57BL6/J genetic background, and heterozygotes in the N7 generation were intercrossed to obtain the homozygotes used in all experiments. STK25 protein was not detected in homozygous mutant mice by Western blotting with an antibody raised against sequences encoded by exon 3 (Supplementary Fig. 1*C*), indicating that the truncated RNA was likely degraded by nonsense-mediated decay. Only male mice were used for phenotyping. From the age of 6 weeks, knockout mice and wild-type littermates were fed a pelleted high-fat diet (45% kilocalories from fat) (D12451; Research Diets, New Brunswick, NJ). Age-matched siblings fed a chow diet were included in most experiments as a reference group. At the age of 26 weeks, the mice were killed after 4 h of food withdrawal. Blood was collected by heart puncture. Epididymal white adipose tissue (eWAT) and liver were weighed. Liver, gastrocnemius skeletal muscle, and subcutaneous white adipose tissue (sWAT) samples were collected for histological analysis (see HISTOLOGY AND IMMUNOFLUORESCENCE) or snap frozen in liquid nitrogen and stored at −80°C for analysis of protein and gene expression. Isolation and size assessment of adipocytes were performed as previously described (7). All animal experiments were performed after approval from the local Ethics Committee for Animal Studies at the Administrative Court of Appeals in Gothenburg, Sweden, and followed appropriate guidelines.

Body Composition and Indirect Calorimetry

Body composition analysis (BCA) of total, lean, and fat body mass was performed in conscious mice by a Bruker minispec LF110 Whole Body Composition Rat and Mice Analyzer (5.7-MHz time domain nuclear magnetic resonance system) (Bruker Corporation, Rheinstetten, Germany). Food intake, total energy expenditure, and respiratory exchange ratio (RER) were assessed using an indirect calorimeter chamber (INCA; SOMEDIC, Hörby, Sweden) as previously described (7).

Blood Chemistry

Four hours after food withdrawal, basal glucose and insulin levels were measured in blood samples taken from the tip of the tail using an Accu-Chek glucometer (Roche Diagnostics, Basel, Switzerland) and Ultra Sensitive Mouse Insulin ELISA Kit (Crystal Chem, Downers Grove, IL), respectively. Plasma triacylglycerol, cholesterol, and ketone levels were measured using a Triglyceride Quantification Colorimetric/Fluorometric Kit (BioVision, Mountain View, CA), cholesterol kit (Sigma-Aldrich, St. Louis, MO), and β-Hydroxybutyrate (Keytone Body) Assay Kit (Cayman Chemical, Ann Arbor, MI), respectively.

Glucose, Pyruvate, and Insulin Tolerance Tests

After 4 h of food withdrawal, mice were injected with glucose (1 g/kg; Fresenius Kabi, Bad Homburg, Germany), sodium pyruvate (2 g/kg; Sigma-Aldrich), or human recombinant insulin (1 unit/kg Actrapid Penfill; Novo Nordisk, Bagsværd, Denmark) intraperitoneally at time 0 for glucose tolerance test (GTT), pyruvate tolerance test (PTT), and insulin tolerance test (ITT), respectively. Blood was taken from the tail tip to determine plasma glucose concentrations at 0, 30, 60, 90, and 120 min postinjection using an Accu-Chek glucometer. The plasma insulin concentration was assessed during GTT at 0, 5, 10, and 30 min after glucose challenge using the Ultra Sensitive Mouse Insulin ELISA Kit. The GTT, PTT, and ITT were performed in mixed groups of knockout mice and wild-type controls at about the same time of day.

Euglycemic-Hyperinsulinemic Clamps

Surgery and glucose and insulin infusion were performed as previously described (7) using an insulin infusion rate

of 7 mU/min/kg. When the steady state was reached (t = ~90 min), a bolus of 2-deoxy-D-[^{14}C]glucose (1.5 μCi; PerkinElmer, Waltham, MA) was injected through the jugular vein. Blood was sampled at 93, 96, 100, 105, 110, 120, 130, and 150 min postinjection. Mice were then killed and tissues analyzed for glucose uptake as previously described (19).

Histology and Immunofluorescence

Liver, gastrocnemius muscle, and sWAT samples were fixed with 4% formaldehyde in phosphate buffer (Histolab Products, Gothenburg, Sweden), embedded in paraffin, sectioned, and stained with hematoxylin-eosin (H-E). Liver samples were also embedded in optimal cutting temperature mounting medium (Histolab Products) and frozen in isopentane cooled by dry ice followed by cryosectioning and Oil Red O staining. Total hepatic lipid area and lipid droplet size distribution and average muscle fiber diameter and fiber size distribution were assessed in five randomly selected 20× microscopic fields per mouse using ImageJ version 1.47 software (National Institutes of Health, Bethesda, MD). For immunofluorescence, gastrocnemius muscle sections were incubated with rabbit anti-perilipin 2 antibody (bs-1164R; Bioss, Woburn, MA) followed by incubation with Alexa Fluor 594–labeled anti-rabbit IgG (A21207; Life Technologies, Grand Island, NY). Quantification of immunofluorescence was based on three randomly selected 10× microscopic fields per mouse.

Analysis of Tissue Glycogen and Lipids

Liver and skeletal muscle glycogen content was determined as previously described (7). Hepatic lipids were extracted using the Folch method (20) and quantified using ultraperformance liquid chromatography/mass spectrometry and direct-infusion mass spectrometry (8).

Western Blot Analysis and Quantitative Real-Time PCR

Western blotting was performed as previously described (21) (see Supplementary Table 1 for antibody information). Quantitative real-time PCR was done using the ABI Prism 7900HT Sequence Detection System (Applied Biosystems, Foster City, CA) as previously described (7).

Ubiquitin Pulldown Assay

An ubiquitinated protein enrichment kit (Calbiochem, San Diego, CA) was used according to the manufacturer's instructions. Briefly, 200 μg total liver protein lysate was tumbled with 40 μL affinity bead suspension overnight at 4°C. After the beads were washed three times in lysis buffer, the sample buffer was added, and the beads were incubated for 5 min at 95°C. Bound proteins were separated by gel electrophoresis and analyzed by Western blot using anti-acetyl-CoA carboxylase (ACC) antibody (see previous paragraph).

Statistical Analysis

Statistical significance between groups was calculated using SPSS version 22 software (IBM Corporation, Armonk, NY) with an unpaired two-tailed Student t test or by two-way ANOVA followed by Tukey post hoc test. $P < 0.05$ was considered statistically significant.

RESULTS

Body Weight and Composition and Food Intake in *Stk25* Knockout Mice

Stk25 mutant mice were generated by deletion of exons 4 and 5, which causes a frameshift and translational termination as previously described (Supplementary Fig. 1) (18). Here, we examined the phenotypic consequences of a high-fat diet challenge (45% kilocalories from fat) on male *Stk25* homozygous mutant ($^{-/-}$) mice and wild-type littermates. In most experiments, chow-fed and sex- and age-matched reference groups were included for *Stk25*$^{-/-}$ and wild-type mice (see Supplementary Fig. 2 for experimental scheme).

Stk25 knockout mice were born at the expected Mendelian ratio and appeared normal by gross inspection. Nose to anus body length was unaffected by depletion of STK25 (Table 1). No difference in body weight was observed between the genotypes fed a high-fat or chow diet (Fig. 1*A*). After the period of high-fat feeding, the total, lean, and fat body mass assessed by BCA as well as the weight of epididymal adipose tissue depots were similar between *Stk25* knockout and wild-type mice (Fig. 1*B* and Table 1). However, on chow diet, the fat body mass and weight of epididymal adipose tissue depots,

Table 1—Body length and weight of adipose tissue depots and liver in *Stk25* KO mice and WT littermates

Parameter	WT CD	KO CD	WT HFD	KO HFD
Body length (cm)	8.98 ± 0.10	9.00 ± 0.11	9.53 ± 0.16††	9.50 ± 0.08##
eWAT (g)	1.57 ± 0.16	1.17 ± 0.13	1.84 ± 0.20	2.10 ± 0.24##
eWAT (% body weight)	4.31 ± 0.36	3.30 ± 0.40*	4.43 ± 0.35	5.18 ± 0.32
Liver (g)	1.38 ± 0.09	1.34 ± 0.07	1.77 ± 0.20	1.57 ± 0.14
Liver (% body weight)	3.80 ± 0.23	3.78 ± 0.19	4.26 ± 0.35	3.87 ± 0.25

Data are mean ± SEM from 10–12 mice per genotype and diet group. The body length and adipose tissue depot and liver weights were estimated in mice fed an HFD for 20 weeks compared with age-matched CD groups. CD, chow diet; HFD, high-fat diet; KO, knockout; WT, wild type. *$P < 0.05$ for *Stk25*$^{-/-}$ mice vs. corresponding WT littermates; ††$P < 0.01$ for WT mice fed HFD vs. CD; ##$P < 0.01$ for *Stk25*$^{-/-}$ mice fed HFD vs. CD.

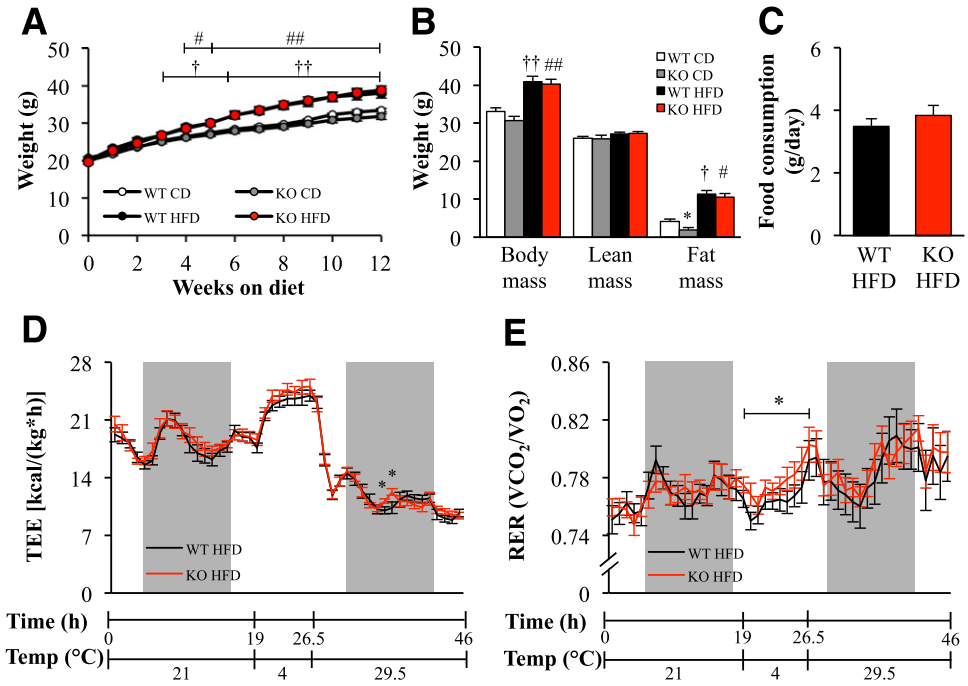

Figure 1—Body weight and composition, food intake, energy expenditure, and substrate utilization in *Stk25* knockout mice and wild-type littermates. *A*: Body weight curves in mice fed a high-fat or chow diet. *B*: Total, lean, and fat body mass measured by BCA in mice fed a high-fat diet for 16 weeks compared with chow-fed groups. *C*: Accumulated food intake per day in mice after 16 weeks of high-fat–diet consumption. *D* and *E*: Total energy expenditure (*D*) and RER (*E*) per hour measured at 21°C, 4°C, and 29.5°C in mice fed a high-fat diet for 16 weeks. The light and dark periods of measurement are labeled. Animals were housed during 48 h, and the data for the first 2 h were discarded to account for acclimatization to the testing conditions. Data are mean ± SEM from 8–13 mice per genotype and diet group. **P* < 0.05 for *Stk25*$^{-/-}$ mice vs. corresponding wild-type littermates; †*P* < 0.05, ††*P* < 0.01 for wild-type mice fed high-fat vs. chow diet; #*P* < 0.05, ##*P* < 0.01 for *Stk25*$^{-/-}$ mice fed high-fat vs. chow diet. CD, chow diet; HFD, high-fat diet; KO, knockout; TEE, total energy expenditure; WT, wild type.

expressed as percent of body weight, were slightly lower in knockout mice than in wild-type controls ($P < 0.05$) (Fig. 1*B* and Table 1). The liver weight was similar between the genotypes in both diet groups (Table 1). Food intake was assessed only in mice fed a high-fat diet, and no difference was found between the genotypes (3.8 ± 0.3 vs. 3.5 ± 0.2 g/day in knockout vs. wild-type mice, respectively) (Fig. 1*C*).

Energy Homeostasis

Oxygen consumption and RER were measured by indirect calorimetry at three different temperatures (4°C, 21°C, and 29.5°C) in mice fed a high-fat diet for 16 weeks. No differences in energy expenditure were found between *Stk25*$^{-/-}$ and wild-type mice at any of the temperatures studied (Fig. 1*D*). No alterations in RER were found between genotypes at 21°C and 29.5°C, suggesting comparable fuel partitioning patterns (Fig. 1*E*). However, a slight increase in RER was observed in *Stk25*$^{-/-}$ mice at 4°C ($P < 0.05$), suggesting a higher relative oxidation of carbohydrates than lipids (Fig. 1*E*).

Glucose and Lipid Homeostasis and Insulin Sensitivity

High-fat dietary stress is known to promote hyperglycemia, hyperinsulinemia, dyslipidemia, glucose intolerance, and insulin resistance in humans as well as in animal models (1,22). The expected increase in fasting blood glucose after 4–12 weeks of high-fat feeding was lower in *Stk25*$^{-/-}$ mice than in wild-type littermates ($P < 0.05$) (Fig. 2*A*). The fasting plasma insulin increased in response to high-fat feeding in both genotypes; however, at 8 and 14 weeks after the start of the diet, the insulin levels remained 1.5 ± 0.1-fold and 1.6 ± 0.1-fold lower, respectively, in the knockout mice ($P < 0.05$) (Fig. 2*B*). A HOMA of insulin resistance (HOMA-IR) was 1.7 ± 0.1-fold lower in knockout mice than in wild-type littermates after 14 weeks on a high-fat diet ($P < 0.05$) (Fig. 2*C*). No difference in systemic glucose or insulin or HOMA-IR was observed between the genotypes fed a chow diet (Fig. 2*A*–*C*). Fasting plasma concentrations of triacylglycerol, cholesterol and ketone bodies were similar between genotypes in both diet groups (Table 2).

In GTT experiments, blood glucose levels returned to normal more rapidly in *Stk25*$^{-/-}$ mice on both diets than in wild-type controls on the same diet ($P < 0.05$) (Fig. 2*D*), revealing a better-preserved glucose tolerance. The plasma insulin response was assessed at different time points during the GTT in mice fed a high-fat diet. No significant difference was found in the peak circulating insulin level observed at 5 min after glucose administration in *Stk25*$^{-/-}$ mice compared with wild-type siblings

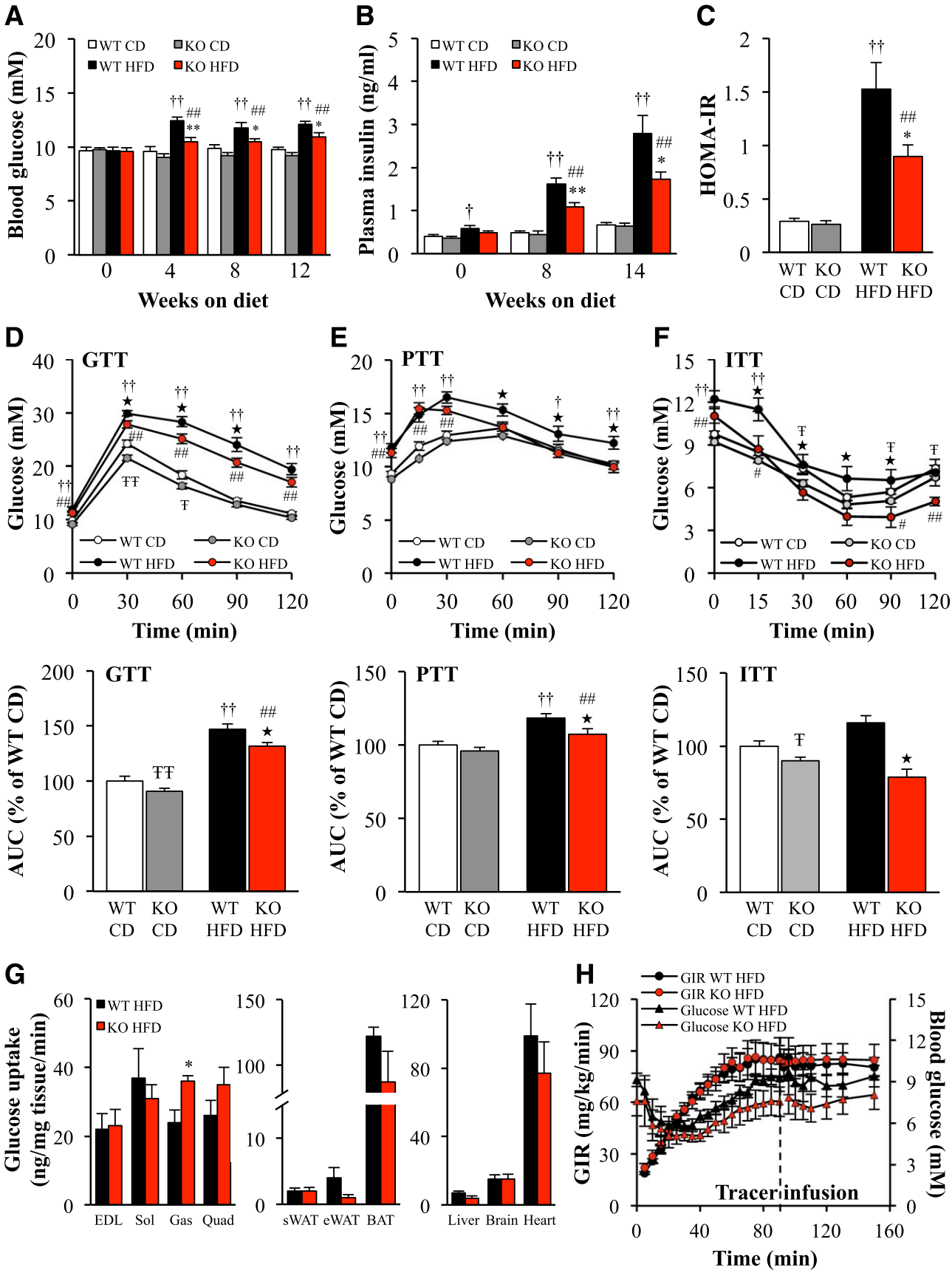

Figure 2—Glucose tolerance and insulin sensitivity in *Stk25* knockout mice and wild-type littermates. *A* and *B*: Fasting circulating levels of glucose (*A*) and insulin (*B*) in mice fed a high-fat or chow diet. *C*: HOMA-IR was calculated using the equation [fasting glucose (mg/dL) ×

(3.0 ± 0.6 ng/mL in knockout mice and 4.0 ± 0.5 ng/mL in wild-type mice).

To determine whether the reduced blood glucose in knockout mice was due to lower hepatic glucose production, we performed a PTT. The challenge with pyruvate, a precursor in the synthesis of glucose during hepatic gluconeogenesis, resulted in lower blood glucose levels in high-fat–fed *Stk25*$^{-/-}$ mice than in wild-type siblings on the same diet ($P < 0.05$), reaching the levels observed in chow-fed mice at 60–120 min postinjection (Fig. 2*E*). No difference in PTT was found between genotypes fed a chow diet (Fig. 2*E*). An ITT revealed marked improvement in insulin sensitivity in *Stk25*$^{-/-}$ mice versus wild-type littermates in both diet groups ($P < 0.05$) (Fig. 2*F*).

Euglycemic-hyperinsulinemic clamps were performed in *Stk25*$^{-/-}$ and wild-type mice fed a high-fat diet for 19 weeks. Insulin infusion markedly increased plasma insulin levels at the end of the clamp for both genotypes (0.9 ± 0.3 vs. 7.7 ± 0.4 ng/mL for basal vs. insulin-stimulated conditions in *Stk25*$^{-/-}$ mice [$P < 0.01$] and 1.5 ± 0.3 vs. 7.8 ± 0.3 ng/mL for basal vs. insulin-stimulated conditions in wild-type mice [$P < 0.01$]), with no significant differences between the genotypes. Insulin-stimulated glucose uptake was 1.4 ± 0.1-fold higher in gastrocnemius muscles of *Stk25*$^{-/-}$ mice compared with wild-type controls ($P < 0.05$), with a similar tendency seen in quadriceps muscle (Fig. 2*G*). No difference in glucose infusion rate at steady state of the clamp was found between the genotypes, which likely relates to the high insulin infusion concentration used in this study, whereas a tendency for lower blood glucose level was observed in *Stk25*$^{-/-}$ mice compared with wild-type littermates during the clamp (Fig. 2*H*).

Lipid Accumulation in Peripheral Tissues

Chronic high-fat exposure promotes hepatic lipid accumulation known as nonalcoholic fatty liver disease (NAFLD) (2). Consistent with this, the liver of wild-type mice fed a high-fat diet for 20 weeks was pale, suggesting increased lipid content (Fig. 3*A*). By contrast, the appearance of the liver of *Stk25*$^{-/-}$ mice challenged with a high-fat diet remained similar to the chow-fed groups (Fig. 3*A*). In line with this observation, histological evaluation demonstrated that pronounced macrovesicular steatosis, accompanied by microvesicular steatosis, developed in the liver of wild-type mice during the high-fat challenge, whereas markedly less lipid accumulation was observed in the liver of high-fat–fed *Stk25*$^{-/-}$ mice (Fig. 3*B*). Indeed, quantification of the total lipid area on liver sections showed a 1.9 ± 0.03-fold reduction in high-fat–fed knockout mice compared with wild-type controls on the same diet ($P < 0.01$) (Fig. 3*C*). Morphometric analysis performed in high-fat–fed mice further demonstrated a shift in the hepatic lipid droplet size distribution, with a lower number of very large droplets (area ≥300 μm^2) in *Stk25* knockout livers compared with wild-type livers (0.97 ± 0.37 vs. 9.03 ± 2.52 droplets/mm^2, $P < 0.01$) (Fig. 3*D*). Consistent with these results, lipidomics analysis revealed that a high-fat diet enhanced the levels of hepatic cholesteryl esters (1.7 ± 0.3-fold, $P < 0.05$), triacylglycerols (1.9 ± 0.4-fold, $P = 0.07$), and diacylglycerols (2.1 ± 0.6-fold, $P = 0.08$) in wild-type livers, whereas no increase was seen in knockout livers (Fig. 3*E* and Supplementary Table 2). Liver phosphatidylcholine and phosphatidylethanolamine, known to decrease in connection to NAFLD and/or nonalcoholic steatohepatitis (23–25), were significantly downregulated in response to high-fat feeding in both genotypes ($P < 0.01$), with a slight but significant increase in knockout mice fed a high-fat diet compared with wild-type mice on the same diet ($P < 0.05$) (Fig. 3*E*). Of note, liver ceramide levels were increased in knockout mice fed a chow diet compared with wild-type littermates on the same diet ($P < 0.05$) (Fig. 3*E* and Supplementary Table 2).

Long-term consumption of high-fat foods is also known to lead to ectopic fat deposits in skeletal muscle (4,5). Here, we stained muscle tissue with perilipin 2 because previous reports have shown that perilipin 2 colocalizes with lipid droplets in skeletal muscle and can be used as a marker for lipid deposition (26,27). Similar to previous studies (26), we observed perilipin 2 staining as visually distinct dots in the central area of the muscle fibers and as an intense signal in the subsarcolemmal region, reflecting accumulation of densely packed lipid droplets (Fig. 4*A*). Perilipin 2 staining in gastrocnemius muscle was 1.7 ± 0.04-fold lower in *Stk25*$^{-/-}$ mice than in wild-type littermates fed a high-fat diet for 20 weeks ($P < 0.01$) (Fig. 4*A*), suggesting reduced lipid accumulation. Fibers of gastrocnemius muscle displayed the

fasting insulin (ng/mL)]/405 in mice fed a high-fat diet for 14 weeks and in age-matched chow-fed controls. *D–F*: Intraperitoneal GTT (*D*), PTT (*E*), and ITT (*F*) in mice fed a high-fat diet for 14, 15, and 16 weeks, respectively, and in chow-fed controls. The area under the glucose curve in each test is shown. *G* and *H*: Insulin-stimulated glucose uptake in individual tissues (*G*) and glucose infusion rate and blood glucose concentration (*H*) determined during a euglycemic-hyperinsulinemic clamp in *Stk25*$^{-/-}$ and wild-type mice after 19 weeks of high-fat–diet consumption. Data are mean ± SEM from 5–13 mice per genotype and diet group. In *A–C* and *G*, *$P < 0.05$, **$P < 0.01$ for *Stk25*$^{-/-}$ mice vs. corresponding wild-type littermates. In *D–F*, ★$P < 0.05$ for *Stk25*$^{-/-}$ mice vs. wild-type littermates fed a high-fat diet; ₸$P < 0.05$, ₸₸$P < 0.01$ for *Stk25*$^{-/-}$ mice vs. wild-type littermates fed a chow diet. In all panels, †$P < 0.05$, ††$P < 0.01$ for wild-type mice fed high-fat vs. chow diet; #$P < 0.05$, ##$P < 0.01$ for *Stk25*$^{-/-}$ mice fed high-fat vs. chow diet. AUC, area under the curve; BAT, brown adipose tissue; CD, chow diet; EDL, extensor digitorum longus; Gas, gastrocnemius muscle; GIR, glucose infusion rate; HFD, high-fat diet; KO, knockout; Quad, quadriceps muscle; Sol, soleus muscle; WT, wild type.

Table 2—Circulating lipid levels and hepatic and skeletal muscle glycogen content in *Stk25* KO mice and WT littermates

Parameter	WT CD	KO CD	WT HFD	KO HFD
Plasma triacylglycerol (mmol/L)	0.19 ± 0.01	0.22 ± 0.02	0.31 ± 0.03††	0.26 ± 0.03
Plasma cholesterol (mmol/L)	2.35 ± 0.08	2.30 ± 0.07	2.46 ± 0.09	2.52 ± 0.06#
Plasma β-hydroxybutyrate (mmol/L)	0.88 ± 0.06	0.87 ± 0.03	0.80 ± 0.04	0.83 ± 0.06
Hepatic glycogen (μg/mg)	1.06 ± 0.06	0.92 ± 0.01*	2.85 ± 0.15††	2.42 ± 0.05*,##
Muscle glycogen (μg/mg)	0.76 ± 0.03	0.64 ± 0.03*	0.55 ± 0.04††	0.43 ± 0.03*,##

Data are mean ± SEM from 10–12 mice per genotype and diet group. The blood lipid levels and tissue glycogen content were measured in mice fed an HFD for 20 weeks compared with age-matched CD groups. CD, chow diet; HFD, high-fat diet; KO, knockout; WT, wild type. *$P < 0.05$ for *Stk25*$^{-/-}$ mice vs. corresponding WT littermates; ††$P < 0.01$ for WT mice fed HFD vs. CD; #$P < 0.05$ for *Stk25*$^{-/-}$ mice fed HFD vs. CD; ##$P < 0.01$ for *Stk25*$^{-/-}$ mice fed HFD vs. CD.

characteristic polygonal shape in *Stk25*$^{-/-}$ and wild-type mice, and no difference was found in average muscle fiber diameter (Fig. 4*B*) or fiber size distribution (Fig. 4*C*) between the genotypes in either diet group.

Increased hepatic glycogen content is reported in mouse models in response to high-fat feeding as well as in patients with T2D (28,29). Consistent with this, we found markedly elevated hepatic glycogen in both genotypes fed a high-fat diet compared with chow-fed controls ($P < 0.01$) (Table 2). Of note, the glycogen levels in the liver and skeletal muscle were significantly reduced in *Stk25*$^{-/-}$ mice compared with wild-type controls in both diet groups ($P < 0.05$) (Table 2).

Adipocyte size was increased in both genotypes fed a high-fat diet for 20 weeks compared with chow-fed littermates ($P < 0.01$) (Fig. 4*D–F*). The size of adipocytes was 10.2 ± 3.1% lower in *Stk25*$^{-/-}$ mice than in wild-type controls on a high-fat diet ($P < 0.05$), whereas no difference was seen between genotypes fed a chow diet (Fig. 4*D–F*).

Expression Profiling in Liver and Skeletal Muscle

To elucidate the molecular mechanisms underlying the metabolic changes in *Stk25*$^{-/-}$ mice, the levels of key regulators of lipid and glucose homeostasis were compared in liver and skeletal muscle from *Stk25*$^{-/-}$ and wild-type mice after 20 weeks of high-fat–diet consumption. ACC is one of the key controllers of the balance of lipid storage versus lipid oxidation. ACC activity is regulated by phosphorylation, where kinases such as AMP-activated protein kinase (AMPK) directly phosphorylate and inactivate ACC (30). We found that the total protein abundance of ACC was 2.4 ± 0.4-fold lower in *Stk25*$^{-/-}$ livers than in wild-type livers ($P < 0.01$) (Fig. 5*A*). The level of phospho-ACC was also reduced 1.5 ± 0.2-fold in knockout livers ($P < 0.05$), but there was an apparent increase in the phospho-ACC/ACC ratio in *Stk25*$^{-/-}$ mice, although this was not significant ($P = 0.11$) (Fig. 5*A*). We next examined the total protein abundance of the upstream kinase AMPK and found that its level was also reduced in knockout livers (1.9 ± 0.2-fold, $P < 0.01$) (Fig. 5*A*). No difference was found in the activated phospho-AMPK, reflecting a trend toward an increased phospho-AMPK/AMPK ratio ($P = 0.095$) (Fig. 5*A*). To further investigate the underlying mechanisms for reduced total protein amount of ACC in *Stk25*$^{-/-}$ livers, we compared the relative abundance of ubiquitinated ACC in the two genotypes. Ubiquitination is an early step for proteins destined for proteosomal degradation, and ubiquitination of ACC has been shown to result in inactivation and degradation of ACC (31). We found that the level of ubiquitinated ACC was 2.1 ± 0.5-fold higher in knockout livers compared with wild-type livers ($P < 0.05$) (Fig. 5*B*) despite the total protein abundance of ACC being markedly lower. Consistent with this, we previously observed that the total protein amount of ACC was higher in the skeletal muscle of *Stk25* transgenic mice, whereas the level of ubiquitinated ACC was significantly lower, compared with wild-type littermates (7). Taken together, these findings indicate that STK25 controls the amount of ACC through regulation of ubiquitination and subsequent degradation of this protein. From a broad panel of hepatic mRNA transcripts of genes involved in lipid and glucose metabolism, only the expression of fatty acid transport protein (*Cd36*) was significantly changed in *Stk25*$^{-/-}$ livers ($P < 0.05$) (Fig. 5*C*).

The total protein abundance or the phosphorylation of ACC and AMPK were not changed in the skeletal muscle of *Stk25*$^{-/-}$ mice compared with wild-type siblings (Fig. 5*D*). Of note, the mRNA levels for the key transporters for glucose uptake into muscle cells *Glut1*, *Glut4*, and hexokinase 2 (*Hk2*) were increased 1.6 ± 0.3-fold, 1.8 ± 0.2-fold, and 1.6 ± 0.2-fold, respectively, in *Stk25*$^{-/-}$ skeletal muscle ($P < 0.05$) (Fig. 5*E*). Furthermore, the expression of two rate-limiting enzymes in lipid oxidation was elevated in *Stk25*$^{-/-}$ skeletal muscle: Carnitine palmitoyltransferase 1 (*Cpt1*), which regulates long-chain fatty acyl-CoA uptake and oxidation in mitochondria, was upregulated 1.6 ± 0.2-fold ($P < 0.05$), whereas fatty acyl-CoA oxidase (*Acox1*), which catalyzes the first step of peroxisomal β-oxidation, was increased 1.5 ± 0.2-fold ($P < 0.05$) (Fig. 5*E*). The components of the mitochondrial tricarboxylic acid cycle citrate synthase (*Cs*) and cytochrome-c (*Cycs*) were upregulated 1.8 ± 0.3-fold and 1.6 ± 0.2-fold, respectively, in *Stk25*$^{-/-}$ skeletal muscle

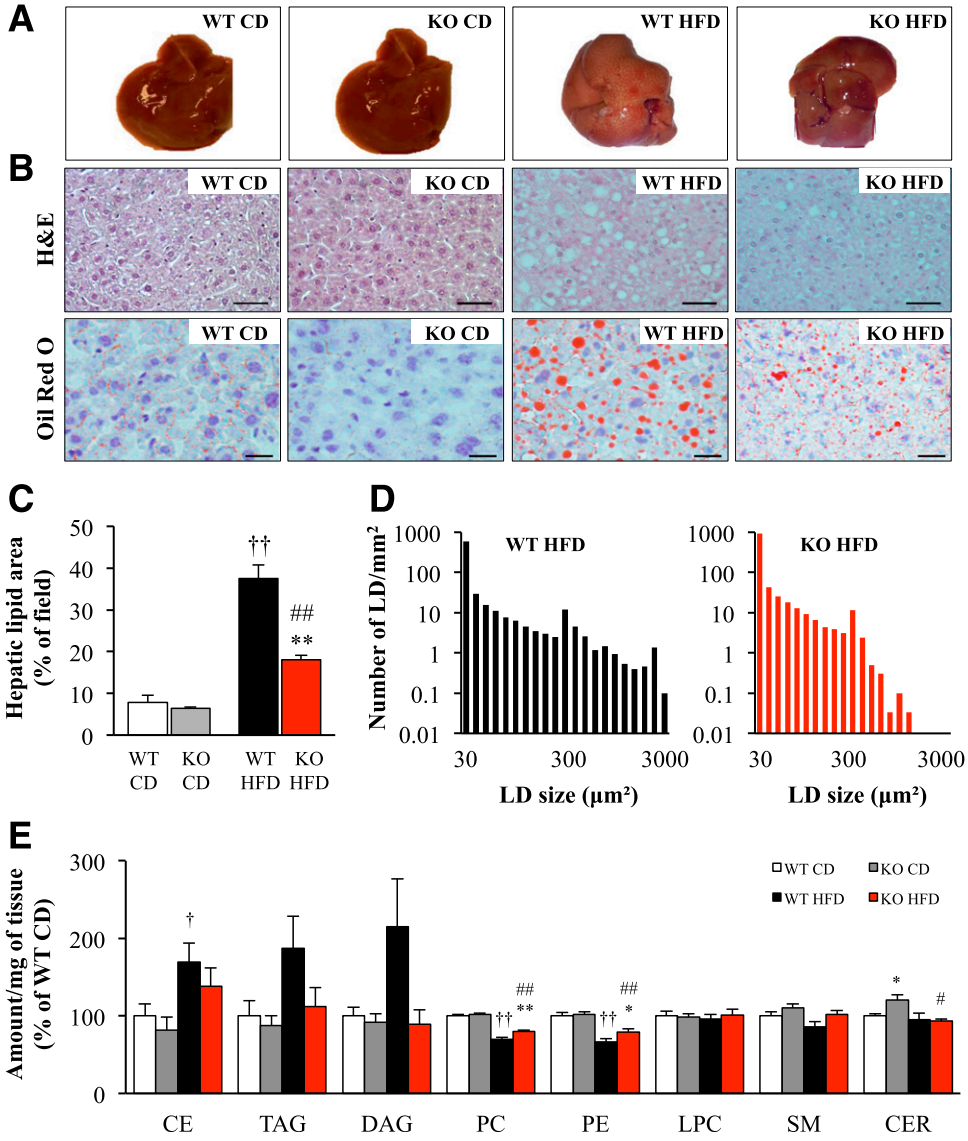

Figure 3—Hepatic lipid deposition in *Stk25* knockout mice and wild-type littermates challenged with a high-fat diet for 20 weeks compared with chow-fed controls. *A*: Representative images of whole liver. *B*: Representative liver sections stained with H-E or Oil Red O for lipids. Scale bar = 100 µm. *C* and *D*: Total lipid area (*C*) and lipid droplet number and size distribution (*D*) in liver sections. *E*: Liver lipid profiling. One outlier, located outside the 99% confidence band, was removed from the analysis. For *C*–*E*, data are mean ± SEM from 6–10 mice per genotype and diet group. **P* < 0.05, ***P* < 0.01 for *Stk25*$^{-/-}$ mice vs. corresponding wild-type littermates; †*P* < 0.05, ††*P* < 0.01 for wild-type mice fed high-fat vs. chow diet; #*P* < 0.05, ##*P* < 0.01 for *Stk25*$^{-/-}$ mice fed high-fat vs. chow diet. CD, chow diet; CE, cholesteryl ester; CER, ceramide; DAG, diacylglycerol; HFD, high-fat diet; KO, knockout; LD, lipid droplet; LPC, lysophosphatidylcholine; PC, phosphatidylcholine; PE, phosphatidylethanolamine; SM, sphingomyelin; TAG, triacylglycerol; WT, wild type.

($P < 0.05$) (Fig. 5*E*). Uncoupling protein 3 (UCP3) is a mitochondrial inner membrane transporter, which has been suggested to facilitate fatty acid oxidation (32). *Ucp3* mRNA was increased 1.7 ± 0.2-fold in *Stk25*$^{-/-}$ skeletal muscle ($P < 0.05$) (Fig. 5*E*). Expression of master transcriptional regulators of fatty acid catabolism peroxisome proliferator–activated receptor α (*Ppara*) and peroxisome proliferator–activated receptor γ, coactivator 1 α (*Ppargc1a*, also known as *Pgc-1α*) was higher but not significantly changed in *Stk25*$^{-/-}$ skeletal muscle (Fig. 5*E*).

DISCUSSION

In this study, we investigated the impact of inactivation of protein kinase STK25 on whole-body metabolism based on phenotypic characterization of *Stk25* knockout mice and wild-type littermates challenged with a high-fat diet. Diet-induced development of hyperglycemia and hyperinsulinemia was suppressed in *Stk25*$^{-/-}$ mice compared with wild-type controls, and knockout mice displayed better-preserved systemic glucose tolerance, reduced hepatic glucose production, and increased insulin sensitivity. Despite these improvements, inactivation of

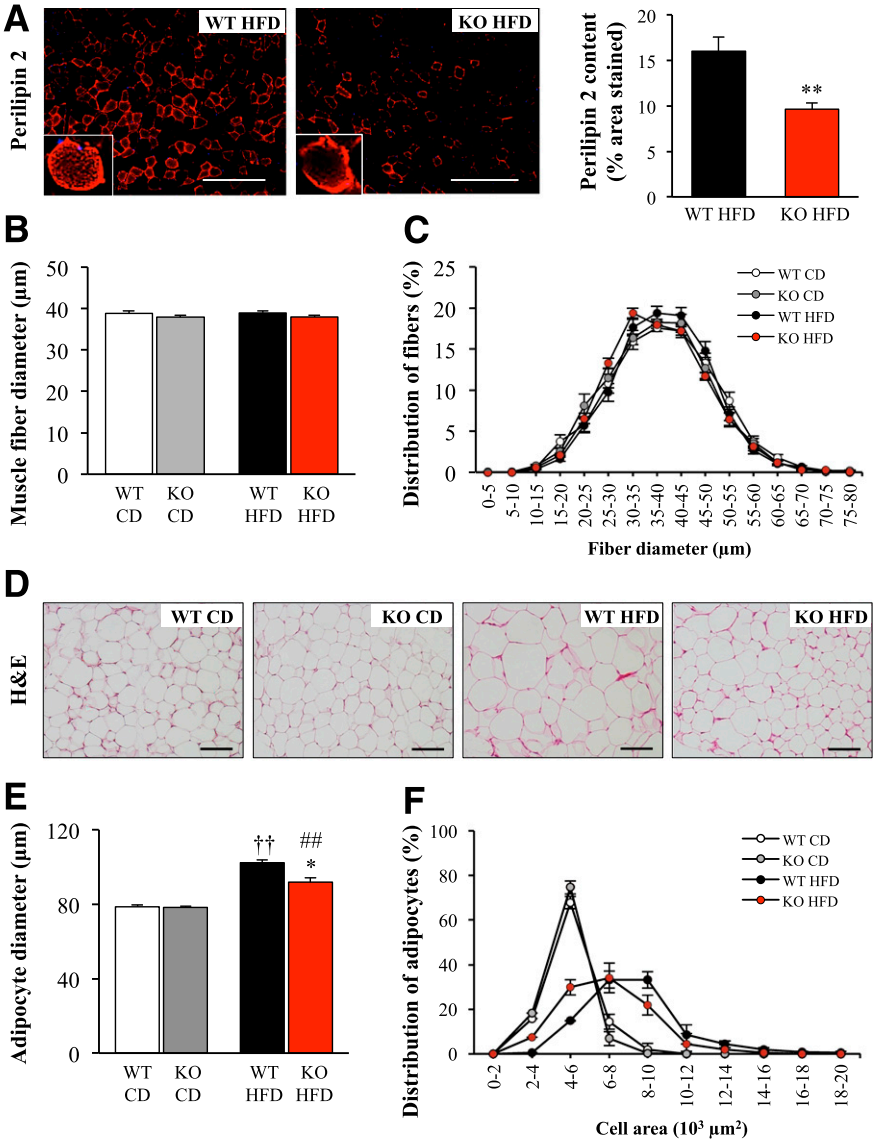

Figure 4—Lipid deposition in skeletal muscle and muscle fiber and adipocyte size distribution in *Stk25* knockout mice and wild-type littermates challenged with a high-fat diet for 20 weeks compared with chow-fed controls. *A*: Representative immunofluorescence images of gastrocnemius skeletal muscle stained with antibodies for perilipin 2 (red) and quantification of perilipin 2 content. Scale bar = 100 μm. *B* and *C*: Average diameter of gastrocnemius skeletal muscle fibers (*B*) and muscle fiber size distribution with values representing the relative proportion of fibers in a given diameter class (*C*). *D*: Representative sections of sWAT depots stained with H-E. Scale bar = 100 μm. *E* and *F*: Average adipocyte diameter (*E*) and adipocyte size distribution with values representing relative proportion of adipocytes in a given diameter class (*F*) in subcutaneous deposits. For *A–C* and *E* and *F*, data are mean ± SEM from 6–9 mice per genotype and diet group. $^{*}P < 0.05$, $^{**}P < 0.01$ for *Stk25*$^{-/-}$ mice vs. corresponding wild-type littermates; ††$P < 0.01$ for wild-type mice fed high-fat vs. chow diet; ##$P < 0.01$ for *Stk25*$^{-/-}$ mice fed high-fat vs. chow diet. CD, chow diet; HFD, high-fat diet; KO, knockout; WT, wild type.

STK25 did not fully ameliorate the progression to diet-induced T2D because the circulating glucose and insulin and glucose tolerance were not restored to levels observed in chow-fed controls. No difference in total, lean, or fat body mass was observed between the genotypes challenged with a high-fat diet, suggesting that inactivation of STK25 protects against the metabolic consequences of chronic exposure to dietary lipids independently of changes in body weight and composition. In contrast to high-fat–fed mice, the fat body mass and the epididymal adipose tissue weight (%) were slightly but significantly lower in chow-fed *Stk25* knockout mice than in corresponding wild-type controls. Although the reason for this difference is not known, the reduced fat mass might have contributed to the improved glucose tolerance and insulin sensitivity observed in chow-fed *Stk25*$^{-/-}$ versus wild-type mice.

Lipid accumulation in liver and skeletal muscle is considered one of the key factors leading to the development of systemic insulin resistance (2–5). Consistent with

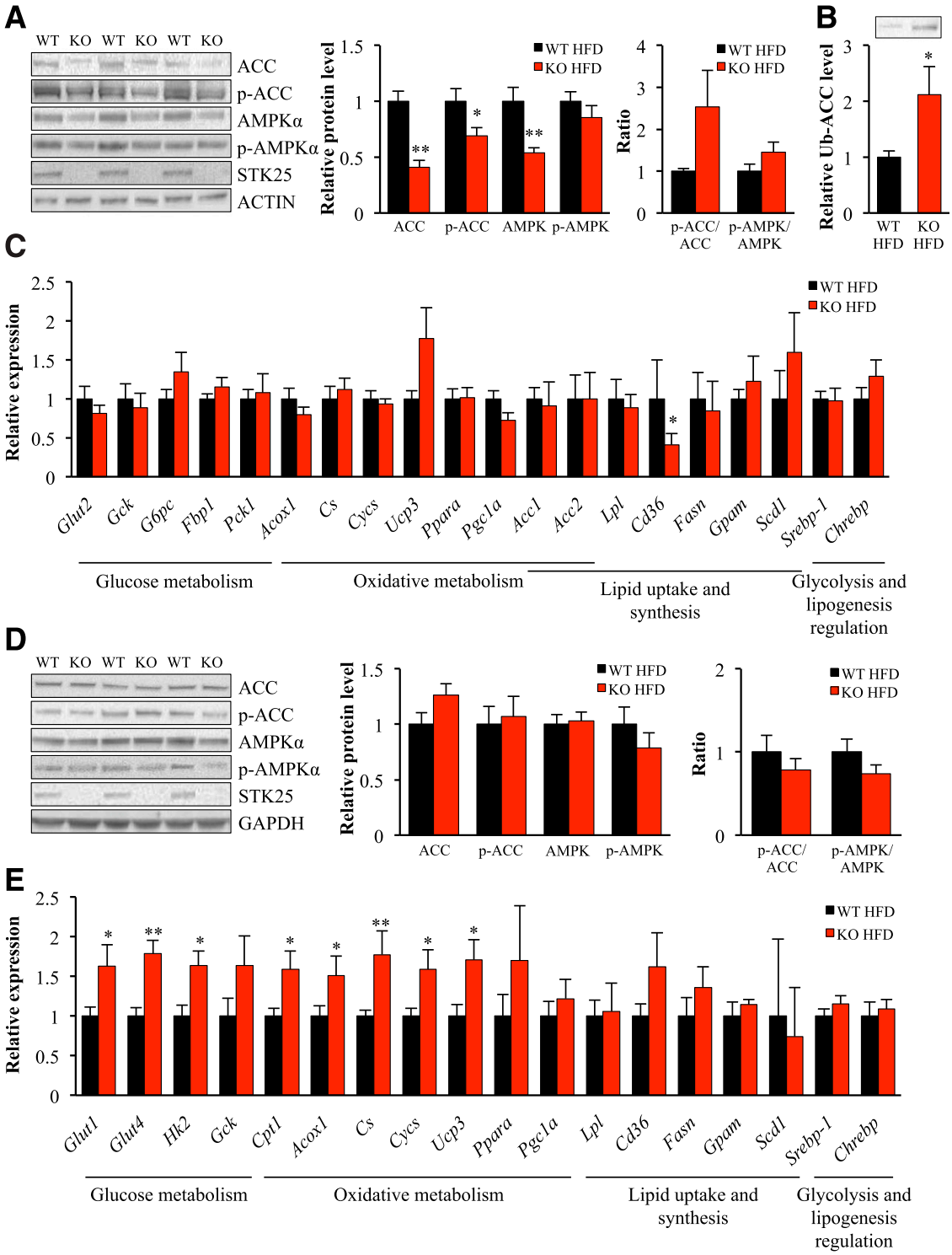

Figure 5—Expression profiling in liver and skeletal muscle of *Stk25* knockout mice and wild-type littermates challenged with a high-fat diet for 20 weeks. *A* and *D*: Protein lysates of the liver (*A*) and gastrocnemius skeletal muscle (*D*) were analyzed by Western blot using antibodies specific for total ACC, phospho-ACC (Ser^{79}), total AMPKα, phospho-AMPKα (Thr^{172}), or STK25. Protein levels were analyzed by densitometry, and data are shown as the total and phospho-protein abundance as well as the ratio of phospho-protein to total protein, with values in wild-type mice set to 1. Representative Western blot is shown with actin (*A*) or glyceraldehyde-3-phosphate dehydrogenase (*D*) used as loading controls. *B*: Protein lysates of liver were enriched for ubiquitinated proteins followed by Western blot using antibodies specific for total ACC. Amount of ubiquitinated ACC was analyzed by densitometry, and the level in wild-type mice was set to 1. *C* and *E*: Relative mRNA expression assessed by quantitative real-time PCR in the liver (*C*) and gastrocnemius skeletal muscle (*E*). The expression level of each selected gene in wild-type mice was set to 1. The gene functions are indicated at the bottom. Data are mean ± SEM from 7–10 mice per genotype. $^{*}P < 0.05$, $^{**}P < 0.01$ for *Stk25*$^{-/-}$ mice vs. wild-type littermates. GAPDH, glyceraldehyde-3-phosphate dehydrogenase; HFD, high-fat diet; KO, knockout; p, phospho; Ub-ACC, ubiquitinated acetyl-CoA carboxylase; WT, wild type.

improved glucose and insulin homeostasis, ectopic lipid storage was markedly lower in the liver and skeletal muscle of *Stk25*$^{-/-}$ mice fed a high-fat diet compared with wild-type controls on the same diet. Of note, ACC protein abundance was significantly reduced in the liver of high-fat–fed *Stk25*$^{-/-}$ versus wild-type mice. ACC regulates both lipogenesis and β-oxidation because its enzymatic product malonyl-CoA is a precursor of fatty acid synthesis and represses lipid oxidation through allosteric inhibition of CPT1 (33). Diet-induced hepatic steatosis can be reversed in mice by reducing ACC expression, which has been attributed to both decreased lipogenesis and increased β-oxidation (33–37). Thus, downregulation of hepatic ACC levels provides a likely mechanism underlying the reduced lipid accumulation in *Stk25*$^{-/-}$ livers. Increased oxidative capacity in the skeletal muscle of high-fat–fed knockout mice, as evidenced by augmented mRNA expression of mitochondrial and peroxisomal enzymes *Cpt1*, *Acox1*, *Cs*, *Cycs*, and *Ucp3*, likely contributed to the decreased lipid storage in the skeletal muscle.

Liver and skeletal muscle glycogen content was reduced in *Stk25*$^{-/-}$ mice on both the high-fat and the chow diet compared with corresponding wild-type controls. Decreased hepatic glycogen has also been reported in *Acc2*$^{-/-}$ mice, which has been attributed to increased utilization of glucose for fatty acid synthesis and their subsequent oxidation (34,38). Similarly, increased oxidative capacity in the liver and skeletal muscle of *Stk25*$^{-/-}$ mice might indirectly contribute to reduced glycogen storage. Because muscle glycogen content is inversely correlated with insulin-stimulated glucose transport (39), reduced muscle glycogen could have contributed to improved glucose tolerance in *Stk25*$^{-/-}$ mice.

LKB1 (liver kinase B1), with its associated factors STRAD and MO25, is the main upstream activator of AMPK (40). STK25 interacts with STRAD and MO25 (11,15), but the impact of this interaction on the function of LKB1 remains unknown. The total protein abundance of AMPK was significantly reduced in *Stk25*$^{-/-}$ livers, but the level of phospho-AMPK, which is the active form, was not changed, suggesting that AMPK is not involved in mediating the metabolic differences between the genotypes.

The energy expenditure at all temperatures tested was comparable between the genotypes fed a high-fat diet. Furthermore, similar RER measurements were observed between *Stk25*$^{-/-}$ and wild-type mice at 21°C and 29.5°C. At 4°C, a slight increase in RER was found in knockout mice, which likely reflects *Stk25*$^{-/-}$ mice not having enough lipids stored in peripheral tissues to support the need for increased lipid oxidation at lower temperatures and during the light phase of observation; therefore, they rely to a larger extent on carbohydrate metabolism.

Discrepancies between acute knockdown versus the conventional knockout phenotypes have been observed for many different genes (41–50) and attributed to compensation for the loss-of-gene function throughout development in knockout mice. By contrast, the current data on the metabolic phenotype of *Stk25* knockout mice are fully consistent with our earlier findings of acute STK25 depletion in the rat myoblast cell line L6 (6). We found increased expression of genes involved in glucose metabolism (*Glut1*, *Glut4*, and *Hk2*) both in L6 cells where STK25 was knocked down by siRNA (6) and in the skeletal muscle of *Stk25*$^{-/-}$ mice. We also previously observed that insulin-stimulated glucose uptake is increased by STK25 knockdown in L6 cells (6) in agreement with the improved glucose tolerance shown in *Stk25*$^{-/-}$ mice in the current study. Similarly, *Ucp3* expression is upregulated both in L6 cells transfected with anti-*Stk25* siRNA (6) and in the skeletal muscle of *Stk25*$^{-/-}$ mice. Of note, although the acute knockdown of STK25 in neuronal cells results in migration disruption and inactivation of STK25 by Cre-mediated excision at E14.5, leading to aberrations in neuronal positioning by E17.5, *Stk25*$^{-/-}$ mice do not display any neuronal phenotype (18). Thus, STK25 depletion early in development leads to full compensation for its role in neuronal function but not in metabolic regulation.

A striking pattern of opposing metabolic alterations is revealed when the phenotype of *Stk25*$^{-/-}$ mice in this study is compared with the previously described phenotype of STK25-overexpressing transgenic mice (7,8). The current observations of decreased hyperinsulinemia, better-preserved systemic glucose tolerance, reduced hepatic gluconeogenesis, and increased insulin sensitivity combined with decreased lipid accumulation in liver and skeletal muscle and reduced adipocyte size in high-fat–fed *Stk25*$^{-/-}$ mice versus wild-type littermates are the reverse of changes we previously showed in high-fat–fed *Stk25* transgenic mice (7,8), which supports the validity of the results (Fig. 6).

A more complex picture emerges when comparing the pattern of gene and protein expression in liver and skeletal muscle between high-fat–fed *Stk25*$^{-/-}$ and *Stk25* transgenic mice. For example, although the protein abundance of ACC is regulated in an opposite manner in *Stk25* knockout versus transgenic liver (7), no alteration in ACC is seen in the skeletal muscle of *Stk25*$^{-/-}$ mice or in L6 cells where STK25 is depleted (6) despite an upregulation in the muscle of transgenic mice (7) (Fig. 6). Furthermore, we observed reciprocal regulation of mRNA expression for *Cpt1* and *Acox1*, two rate-limiting enzymes in lipid oxidation, in *Stk25*$^{-/-}$ versus transgenic skeletal muscle (7) (Fig. 6). However, although we found a coordinated increase in expression of additional enzymes controlling the oxidative capacity (*Cs*, *Cycs*, *Ucp3*) and glucose metabolism (*Glut1*, *Glut4*, *Hk2*) in *Stk25*$^{-/-}$ muscle in this study, opposite changes for these genes were not seen in transgenic muscle (7). Moreover, our previous observation of enhanced expression of key enzymes regulating lipogenesis (fatty acid synthase [*Fasn*]), glycogen synthesis (glucokinase [*Gck*]), and gluconeogenesis (glucose-6-phosphatase [*G6pc*] and fructose-1,6-bisphosphatase [*Fbp1*]) in *Stk25* transgenic livers (7) was not matched by a reciprocal decrease in

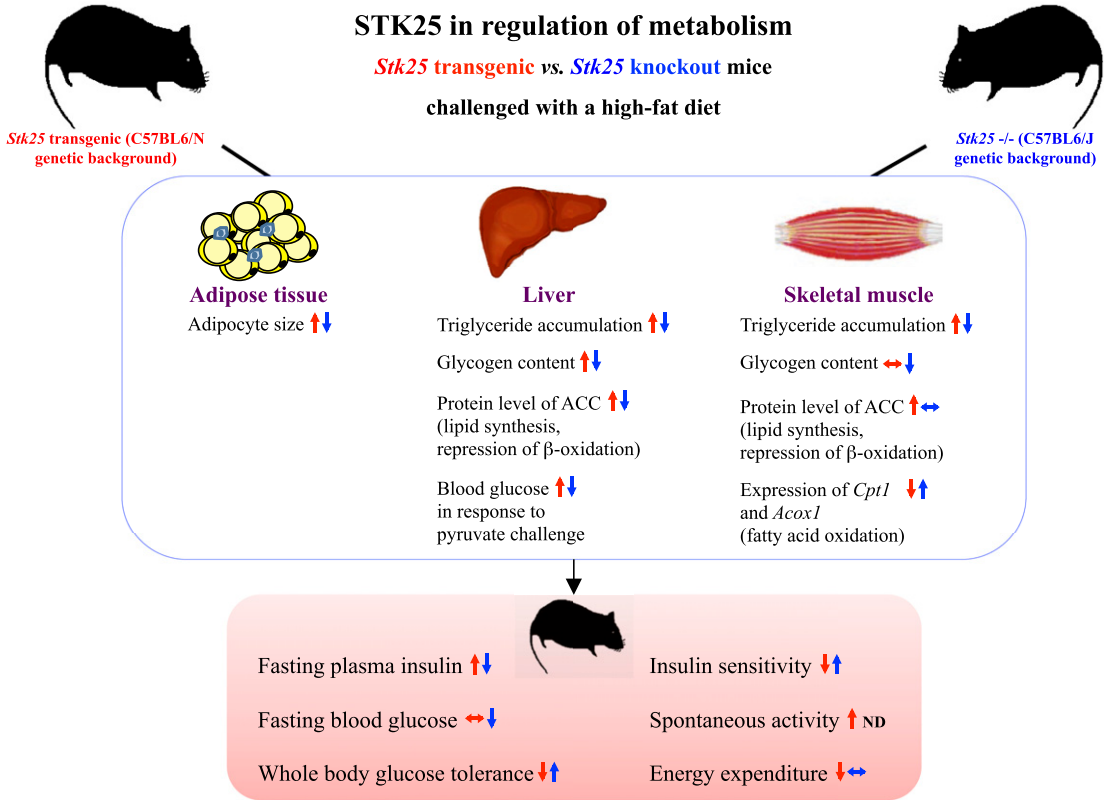

Figure 6—Schematic illustration of reciprocal metabolic responses in individual organs as well as at the whole-body level in *Stk25*$^{-/-}$ mice (indicated by blue arrows) and transgenic mice overexpressing STK25 (indicated by red arrows) compared with corresponding wild-type littermates. The phenotype of *Stk25* transgenic mice has been described previously (7,8). ND, not determined.

expression of these genes in *Stk25*$^{-/-}$ livers. At present, we cannot explain the mechanisms through which STK25 controls metabolic gene expression. However, the variability of the findings between tissues suggests a possibility that tissue-specific functional compensation and different critical thresholds for STK25 exist. Importantly, the global overexpression and depletion of STK25 in transgenic and knockout mice, respectively, do not allow us to address whether the effect of STK25 on liver and skeletal muscle is a direct result of or secondary to the action of STK25 in other tissues, which is a limitation of the models used.

Taken together, the data show that inactivation of STK25 in knockout mice provides substantial protection from the detrimental metabolic consequences of high-fat-diet exposure on liver and skeletal muscle lipid deposition accompanied by reduced circulating glucose and insulin levels and improved whole-body glucose tolerance and insulin sensitivity. The data are highly consistent with previous observations in myoblast cells in which STK25 expression was knocked down (6) and reciprocal to the metabolic phenotype of STK25-overexpressing transgenic mice (7,8), which further reinforces the validity of the findings. Moreover, higher STK25 expression has been observed in skeletal muscle from patients with T2D compared with healthy subjects with normal glucose tolerance (6). The data suggest that antagonists of STK25 may be effective therapeutics for NAFLD, T2D, and related metabolic complications.

Acknowledgments. The authors acknowledge the editorial assistance of Rosie Perkins, Wallenberg Laboratory, Department of Molecular and Clinical Medicine, University of Gothenburg, Gothenburg, Sweden.

Funding. This work was supported by grants from the Swedish Research Council, a European Foundation for the Study of Diabetes/Lilly research grant, the European Foundation for the Study of Diabetes and Novo Nordisk Partnership for Diabetes Research in Europe, the Novo Nordisk Foundation, the Swedish Heart and Lung Foundation, the Diabetes Wellness Network Sweden, the Swedish Diabetes Foundation, the Petrus and Augusta Hedlunds Foundation, the Åke Wiberg Foundation, the Adlerbert Research Foundation, the Magnus Bergvalls Foundation, the Inger Hultman Foundation, and National Institute of Neurological Disorders and Stroke grant NS-073662 (to B.W.H.).

Duality of Interest. No potential conflicts of interest relevant to this article were reported.

Author Contributions. M.A. generated the bulk of the results and reviewed and edited the manuscript. E.C., U.C., and B.C. contributed to the research data and reviewed and edited the manuscript. E.N.-D. and L.M.-H. performed the euglycemic-hyperinsulinemic clamp experiment and reviewed and edited the manuscript. M.S. performed the lipidomics analysis and reviewed and edited the manuscript. V.F. and A.W. conducted the indirect calorimetry and BCAs and reviewed and edited the manuscript. U.S., F.B., and J.B. provided advice and expertise, contributed to the discussion, and reviewed and edited the manuscript. B.W.H. provided advice and reagents and reviewed and edited the manuscript. M.M. directed the project; designed the study; interpreted the

data; and wrote, reviewed, and edited the manuscript. M.M. is the guarantor of this work and, as such, had full access to all the data in the study and takes responsibility for the integrity of the data and the accuracy of the data analysis.

References

1. Hu FB. Globalization of diabetes: the role of diet, lifestyle, and genes. Diabetes Care 2011;34:1249–1257
2. Anstee QM, Targher G, Day CP. Progression of NAFLD to diabetes mellitus, cardiovascular disease or cirrhosis. Nat Rev Gastroenterol Hepatol 2013;10:330–344
3. Perry RJ, Samuel VT, Petersen KF, Shulman GI. The role of hepatic lipids in hepatic insulin resistance and type 2 diabetes. Nature 2014;510:84–91
4. Goodpaster BH, Wolf D. Skeletal muscle lipid accumulation in obesity, insulin resistance, and type 2 diabetes. Pediatr Diabetes 2004;5:219–226
5. Perseghin G, Scifo P, De Cobelli F, et al. Intramyocellular triglyceride content is a determinant of in vivo insulin resistance in humans: a ^{1}H-^{13}C nuclear magnetic resonance spectroscopy assessment in offspring of type 2 diabetic parents. Diabetes 1999;48:1600–1606
6. Nerstedt A, Cansby E, Andersson CX, et al. Serine/threonine protein kinase 25 (STK25): a novel negative regulator of lipid and glucose metabolism in rodent and human skeletal muscle. Diabetologia 2012;55:1797–1807
7. Cansby E, Amrutkar M, Manneras Holm L, et al. Increased expression of STK25 leads to impaired glucose utilization and insulin sensitivity in mice challenged with a high-fat diet. FASEB J 2013;27:3660–3671
8. Amrutkar M, Cansby E, Nunez-Duran E, et al. Protein kinase STK25 regulates hepatic lipid partitioning and progression of liver steatosis and NASH. FASEB J 2015;29:1564–1576
9. Osada S, Izawa M, Saito R, et al. YSK1, a novel mammalian protein kinase structurally related to Ste20 and SPS1, but is not involved in the known MAPK pathways. Oncogene 1997;14:2047–2057
10. Sugden PH, McGuffin LJ, Clerk A. SOcK, MiSTs, MASK and STicKs: the GCKIII (germinal centre kinase III) kinases and their heterologous protein-protein interactions. Biochem J 2013;454:13–30
11. Hao Q, Feng M, Shi Z, et al. Structural insights into regulatory mechanisms of MO25-mediated kinase activation. J Struct Biol 2014;186:224–233
12. Preisinger C, Short B, De Corte V, et al. YSK1 is activated by the Golgi matrix protein GM130 and plays a role in cell migration through its substrate 14-3-3zeta. J Cell Biol 2004;164:1009–1020
13. Fidalgo M, Fraile M, Pires A, Force T, Pombo C, Zalvide J. CCM3/PDCD10 stabilizes GCKIII proteins to promote Golgi assembly and cell orientation. J Cell Sci 2010;123:1274–1284
14. Voss K, Stahl S, Schleider E, et al. CCM3 interacts with CCM2 indicating common pathogenesis for cerebral cavernous malformations. Neurogenetics 2007;8:249–256
15. Matsuki T, Matthews RT, Cooper JA, et al. Reelin and Stk25 have opposing roles in neuronal polarization and dendritic Golgi deployment. Cell 2010;143:826–836
16. Nogueira E, Fidalgo M, Molnar A, et al. SOK1 translocates from the Golgi to the nucleus upon chemical anoxia and induces apoptotic cell death. J Biol Chem 2008;283:16248–16258
17. Zhou J, Shao Z, Kerkela R, et al. Serine 58 of 14-3-3zeta is a molecular switch regulating ASK1 and oxidant stress-induced cell death. Mol Cell Biol 2009;29:4167–4176
18. Matsuki T, Chen J, Howell BW. Acute inactivation of the serine-threonine kinase Stk25 disrupts neuronal migration. Neural Dev 2013;8:21
19. Burcelin R, Dolci W, Thorens B. Glucose sensing by the hepatoportal sensor is GLUT2-dependent: in vivo analysis in GLUT2-null mice. Diabetes 2000;49:1643–1648
20. Folch J, Lees M, Sloane Stanley GH. A simple method for the isolation and purification of total lipides from animal tissues. J Biol Chem 1957;226:497–509
21. Nerstedt A, Johansson A, Andersson CX, Cansby E, Smith U, Mahlapuu M. AMP-activated protein kinase inhibits IL-6-stimulated inflammatory response in human liver cells by suppressing phosphorylation of signal transducer and activator of transcription 3 (STAT3). Diabetologia 2010;53:2406–2416
22. Surwit RS, Kuhn CM, Cochrane C, McCubbin JA, Feinglos MN. Diet-induced type II diabetes in C57BL/6J mice. Diabetes 1988;37:1163–1167
23. Eisinger K, Krautbauer S, Hebel T, et al. Lipidomic analysis of the liver from high-fat diet induced obese mice identifies changes in multiple lipid classes. Exp Mol Pathol 2014;97:37–43
24. Puri P, Baillie RA, Wiest MM, et al. A lipidomic analysis of nonalcoholic fatty liver disease. Hepatology 2007;46:1081–1090
25. Li Z, Agellon LB, Allen TM, et al. The ratio of phosphatidylcholine to phosphatidylethanolamine influences membrane integrity and steatohepatitis. Cell Metab 2006;3:321–331
26. MacPherson REK, Herbst EAF, Reynolds EJ, Vandenboom R, Roy BD, Peters SJ. Subcellular localization of skeletal muscle lipid droplets and PLIN family proteins OXPAT and ADRP at rest and following contraction in rat soleus muscle. Am J Physiol Regul Integr Comp Physiol 2012;302:R29–R36
27. Prats C, Donsmark M, Qvortrup K, et al. Decrease in intramuscular lipid droplets and translocation of HSL in response to muscle contraction and epinephrine. J Lipid Res 2006;47:2392–2399
28. Lu B, Bridges D, Yang Y, et al. Metabolic crosstalk: molecular links between glycogen and lipid metabolism in obesity. Diabetes 2014;63:2935–2948
29. Clore JN, Post EP, Bailey DJ, Nestler JE, Blackard WG. Evidence for increased liver glycogen in patients with noninsulin-dependent diabetes mellitus after a 3-day fast. J Clin Endocrinol Metab 1992;74:660–666
30. Winder WW, Hardie DG. Inactivation of acetyl-CoA carboxylase and activation of AMP-activated protein kinase in muscle during exercise. Am J Physiol 1996;270:E299–E304
31. Qi L, Heredia JE, Altarejos JY, et al. TRB3 links the E3 ubiquitin ligase COP1 to lipid metabolism. Science 2006;312:1763–1766
32. MacLellan JD, Gerrits MF, Gowing A, Smith PJ, Wheeler MB, Harper ME. Physiological increases in uncoupling protein 3 augment fatty acid oxidation and decrease reactive oxygen species production without uncoupling respiration in muscle cells. Diabetes 2005;54:2343–2350
33. Savage DB, Choi CS, Samuel VT, et al. Reversal of diet-induced hepatic steatosis and hepatic insulin resistance by antisense oligonucleotide inhibitors of acetyl-CoA carboxylases 1 and 2. J Clin Invest 2006;116:817–824
34. Abu-Elheiga L, Matzuk MM, Abo-Hashema KA, Wakil SJ. Continuous fatty acid oxidation and reduced fat storage in mice lacking acetyl-CoA carboxylase 2. Science 2001;291:2613–2616
35. Abu-Elheiga L, Oh W, Kordari P, Wakil SJ. Acetyl-CoA carboxylase 2 mutant mice are protected against obesity and diabetes induced by high-fat/high-carbohydrate diets. Proc Natl Acad Sci U S A 2003;100:10207–10212
36. Mao J, DeMayo FJ, Li H, et al. Liver-specific deletion of acetyl-CoA carboxylase 1 reduces hepatic triglyceride accumulation without affecting glucose homeostasis. Proc Natl Acad Sci U S A 2006;103:8552–8557
37. Fullerton MD, Galic S, Marcinko K, et al. Single phosphorylation sites in Acc1 and Acc2 regulate lipid homeostasis and the insulin-sensitizing effects of metformin. Nat Med 2013;19:1649–1654
38. Choi CS, Savage DB, Abu-Elheiga L, et al. Continuous fat oxidation in acetyl-CoA carboxylase 2 knockout mice increases total energy expenditure, reduces fat mass, and improves insulin sensitivity. Proc Natl Acad Sci U S A 2007;104:16480–16485
39. Derave W, Lund S, Holman GD, Wojtaszewski J, Pedersen O, Richter EA. Contraction-stimulated muscle glucose transport and GLUT-4 surface content are dependent on glycogen content. Am J Physiol 1999;277:E1103–E1110
40. Ruderman NB, Carling D, Prentki M, Cacicedo JM. AMPK, insulin resistance, and the metabolic syndrome. J Clin Invest 2013;123:2764–2772
41. Chang BHJ, Li L, Paul A, et al. Protection against fatty liver but normal adipogenesis in mice lacking adipose differentiation-related protein. Mol Cell Biol 2006;26:1063–1076
42. Varela GM, Antwi DA, Dhir R, et al. Inhibition of ADRP prevents diet-induced insulin resistance. Am J Physiol Gastrointest Liver Physiol 2008;295:G621–G628

43. Bai J, Ramos RL, Paramasivam M, Siddiqi F, Ackman JB, LoTurco JJ. The role of DCX and LIS1 in migration through the lateral cortical stream of developing forebrain. Dev Neurosci 2008;30:144–156
44. Corbo JC, Deuel TA, Long JM, et al. Doublecortin is required in mice for lamination of the hippocampus but not the neocortex. J Neurosci 2002;22:7548–7557
45. Deuel TA, Liu JS, Corbo JC, Yoo SY, Rorke-Adams LB, Walsh CA. Genetic interactions between doublecortin and doublecortin-like kinase in neuronal migration and axon outgrowth. Neuron 2006;49:41–53
46. Koizumi H, Tanaka T, Gleeson JG. Doublecortin-like kinase functions with doublecortin to mediate fiber tract decussation and neuronal migration. Neuron 2006;49:55–66
47. Zheng H, Jiang M, Trumbauer ME, et al. β-Amyloid precursor protein-deficient mice show reactive gliosis and decreased locomotor activity. Cell 1995; 81:525–531
48. Young-Pearse TL, Bai J, Chang R, Zheng JB, LoTurco JJ, Selkoe DJ. A critical function for beta-amyloid precursor protein in neuronal migration revealed by in utero RNA interference. J Neurosci 2007;27:14459–14469
49. Chou WH, Choi DS, Zhang H, et al. Neutrophil protein kinase Cdelta as a mediator of stroke-reperfusion injury. J Clin Invest 2004;114:49–56
50. Zhao CT, Li K, Li JT, et al. PKCdelta regulates cortical radial migration by stabilizing the Cdk5 activator p35. Proc Natl Acad Sci U S A 2009;106:21353–21358